Missouri University of Science and Technology
Scholars' Mine

Physics Faculty Research & Creative Works | Physics

01 Oct 2003

Perturbation Approach to the Self-Energy of Non-S Hydrogenic States

Eric Olivier Le Bigot

Ulrich D. Jentschura
Missouri University of Science and Technology, ulj@mst.edu

Peter J. Mohr

Paul Indelicato

et. al. For a complete list of authors, see https://scholarsmine.mst.edu/phys_facwork/850

Follow this and additional works at: https://scholarsmine.mst.edu/phys_facwork

 Part of the Physics Commons

Recommended Citation

E. O. Le Bigot et al., "Perturbation Approach to the Self-Energy of Non-S Hydrogenic States," *Physical Review A - Atomic, Molecular, and Optical Physics*, vol. 68, American Physical Society (APS), Oct 2003. The definitive version is available at https://doi.org/10.1103/PhysRevA.68.042101

This Article - Journal is brought to you for free and open access by Scholars' Mine. It has been accepted for inclusion in Physics Faculty Research & Creative Works by an authorized administrator of Scholars' Mine. This work is protected by U. S. Copyright Law. Unauthorized use including reproduction for redistribution requires the permission of the copyright holder. For more information, please contact scholarsmine@mst.edu.

Perturbation approach to the self-energy of non-*S* hydrogenic states

Eric-Olivier Le Bigot,[1,2] Ulrich D. Jentschura,[1,2,3] Peter J. Mohr,[2] Paul Indelicato,[1] and Gerhard Soff[3]
[1]*Laboratoire Kastler Brossel, École Normale Supérieure et Université Pierre et Marie Curie, Case 74, 75005 Paris, France*
[2]*National Institute of Standards and Technology, Mail Stop 8401, Gaithersburg, Maryland 20899-8401, USA*
[3]*Institut für Theoretische Physik, Technische Universität Dresden, 01062 Dresden, Germany*
(Received 8 April 2003; published 3 October 2003)

We present results on the self-energy correction to the energy levels of hydrogen and hydrogenlike ions. The self-energy represents the largest QED correction to the relativistic (Dirac-Coulomb) energy of a bound electron. We focus on the perturbation expansion of the self-energy of non-*S* states, and provide estimates of the so-called A_{60} perturbation coefficient, which can be viewed as a relativistic Bethe logarithm. Precise values of A_{60} are given for many *P*, *D*, *F*, and *G* states, while estimates are given for other states. These results can be used in high-precision spectroscopy experiments in hydrogen and hydrogenlike ions. They yield the best available estimate of the self-energy correction of many atomic states.

DOI: 10.1103/PhysRevA.68.042101 PACS number(s): 12.20.Ds, 31.30.Jv, 06.20.Jr, 31.15.−p

I. INTRODUCTION

The recent dramatic progress in high-precision spectroscopy (see, e.g., Ref. [1]) has motivated the calculation of numerous contributions to the energy levels of hydrogen and hydrogenlike systems. Such spectroscopic experiments test our understanding of atomic levels and provide precise determinations of fundamental constants [2]; this requires accurate predictions of atomic energies and, in particular, the calculation of corrections due to quantum electrodynamics (QED), the quantum field theory of electromagnetic interactions. The largest correction to the relativistic (Dirac) energy levels of hydrogen and hydrogenlike ions is provided by the so-called *self-energy* contribution of QED. The self-energy is a process which modifies the relativistic (Dirac) energy of an electron, and can be depicted by the following Feynman diagram:

where the double line denotes the electron (bound to the nucleus) and the wavy line represents the photon emitted and reabsorbed by the electron. The self-energy correction to energy levels in hydrogen and hydrogenlike ions can be expressed as an expansion in $Z\alpha$ and $\ln(Z\alpha)$ (see, e.g., Ref. [3]), where Z is the nuclear charge number of the nucleus of the hydrogenlike ion under consideration and α is the fine-structure constant. Analytic calculations of the (one-loop) self-energy in bound systems have a long history, starting from Bethe's seminal paper [4], and have since extended over more than five decades.

The purpose of this paper is to provide good approximate values of the self-energy correction to the energy levels of hydrogen and hydrogenlike ions for any *P* state and any state with a higher angular momentum. Only a part of the perturbation expansion of the self-energy of these states is known analytically. The first two contributions to this expansion that are not known in closed analytic form are the Bethe logarithm $\ln k_0(nl)$ and the so-called $A_{60}(nl_j)$ coefficient of the self-energy, which can be characterized as a *relativistic* Bethe logarithm [see Sec. II, and in particular Eqs. (1), (7), and (8)]. Here, nl_j is the standard spectroscopic notation for an atomic state. This paper thus contains numerical values of A_{60}, as well as formulas for estimating both of these important quantities for high l (see Secs. V and VI).

Very precise numerical values of the Bethe logarithm $\ln k_0(nl)$ have been obtained (see, e.g., Refs. [5,6]), and numerical convergence acceleration techniques [7] can yield very precise values of this quantity for any atomic state nl. The estimate (37) that we obtained as a by-product in Sec. VI should be useful to experiments that use high-l levels for which no published values of the Bethe logarithm exist (see, e.g., Ref. [8]).

Many new values of the relativistic Bethe logarithm $A_{60}(nl_j)$ have recently been published [9]. Other values have been obtained previously for some *S* [10–12] and *P* states [13,14]. This paper contains two additional values [$A_{60}(5F_{5/2})$ and $A_{60}(5F_{7/2})$], as well as details of the procedure that we used in obtaining the values of A_{60} in Ref. [9] and in Table III (see Sec. IV).

The results of Secs. IV–VI provide an improvement over the available approximations of the bound-electron self-energy, over a large range of nuclear charge numbers *Z*. In particular, they yield the best available estimates for the self-energy correction in hydrogen, for all the states for which no exact (nonperturbative) value of the self-energy has yet been published (i.e., all levels, except $n=1$ and $n=2$ levels [12,15]).

It is important to know accurately the energy (and in particular the self-energy) of higher angular-momentum states, because they are used in high-precision spectroscopic measurements [16–21]. States with very high angular orbital quantum numbers $l \simeq 30$ have been recently used in such experiments [8]. Further motivation for the present study results from the need to accurately compare the two approaches that have been used for the theoretical study of QED shifts, so as to check their consistency: (i) the analytic expansion in the parameter $Z\alpha$, mostly used for low-Z systems, and (ii) the numerical approach which avoids the $Z\alpha$ expansion and has been used predominantly for the theoretical description of high-Z hydrogenlike ions [22].

Recently, the most accurate methods implementing a non-

 ©2003 The American Physical Society

TABLE I. Self-energy coefficient A_{60} for P states [see Eq. (7)]. The quoted error is due to numerical integration. As in previous calculations (see Refs. [13,14]), certain remaining one-dimensional integrals involving (partial derivatives of) hypergeometric functions could only be evaluated numerically.

n	$P_{1/2}$ ($\kappa=1$)	$P_{3/2}$ ($\kappa=-2$)
2	−0.998 904 402(1)	−0.503 373 465(1)
3	−1.148 189 956(1)	−0.597 569 388(1)
4	−1.195 688 142(1)	−0.630 945 795(1)
5	−1.216 224 512(1)	−0.647 013 508(1)
6	−1.226 702 391(1)	−0.656 154 893(1)
7	−1.232 715 957(1)	−0.662 027 568(1)

perturbative calculation of the self-energy [15,23–26] have been extended by analytic results [27]. Taken together, they provide access to the self-energy shift of electrons of total angular momentum $j>3/2$. This has allowed us to obtain numerical values of the self-energy, and to use them in *checks* of the A_{60} coefficients presented in Tables I–IV (see Sec. VII).

Moreover, general progress in theoretical calculations of atomic energy levels has been achieved by means of numerical algorithms [7,26,28] that lead to an accelerated convergence of the angular-momentum series expansion of the bound-electron relativistic Green function. Such algorithms are also useful for performing the series summations that we had to do in order to obtain the values of A_{60} presented here (see Sec. IV).

Notation and conventions are defined in Sec. II. The mathematical method used for the semianalytic calculations of A_{60} in Ref. [9] is discussed in Sec. III. Details of these calculations for P, D, F, and G states are presented in Sec. IV (numerical results are presented in Tables I–IV). Approximate formulas for the relativistic Bethe logarithm $A_{60}(nl_j)$ of P and D states with high n are presented in Sec. V. Estimates of the Bethe logarithm $\ln k_0(nl)$ and of $A_{60}(nl_j)$ as a function of the orbital quantum number l are reported in Sec. VI. We have performed additional checks of the values of A_{60} in Tables I–IV, as described in Sec. VII; we also show in this section that for the states considered here, the inclusion of A_{60} in the (truncated) perturbation expansion of the electron self-energy [Eq. (7) below] does indeed improve the self-energy estimates. A summary of the paper is given in Sec. VIII. The fitting method that we used in obtaining asymptotic behaviors of $\ln k_0(nl)$ and of $A_{60}(nl_j)$ is described in the Appendix.

TABLE II. A_{60} coefficients for D states.

n	$D_{3/2}$ ($\kappa=2$)	$D_{5/2}$ ($\kappa=-3$)
3	0.005 551 573(1)	0.027 609 989(1)
4	0.005 585 985(1)	0.031 411 862(1)
5	0.006 152 175(1)	0.033 077 570(1)
6	0.006 749 745(1)	0.033 908 493(1)
7	0.007 277 403(1)	0.034 355 926(1)
8	0.007 723 850(1)	0.034 607 492(1)

TABLE III. A_{60} coefficients for F states.

n	$F_{5/2}$ ($\kappa=3$)	$F_{7/2}$ ($\kappa=-4$)
4	0.002 326 988(1)	0.007 074 961(1)
5	0.002 403 158(1)	0.008 087 020(1)

II. NOTATION AND CONVENTIONS

In this section, we define the notation and conventions used in this paper. We write the (real part of the) one-loop self-energy shift of an electron in the level n with orbital angular momentum l and total angular momentum j as

$$\Delta E_{\mathrm{SE}}=\frac{\alpha}{\pi}\frac{(Z\alpha)^4}{n^3}F(nl_j,Z\alpha)mc^2, \tag{1}$$

where $F(nl_j,Z\alpha)$ is a dimensionless quantity. We use natural units, in which $\hbar=c=m=1$ (m is the electron mass). It is customary in the literature to suppress the dependence of F on the quantum numbers n, j, and l and write $F(Z\alpha)$ for $F(nl_j,Z\alpha)$.

The quantum numbers l and j can be combined into the Dirac angular quantum number κ. As a function of j and l, κ is given by

$$\kappa=2(l-j)(j+1/2), \tag{2a}$$

i.e.,

$$\kappa=-(j+1/2) \quad \text{for} \quad j=l+1/2 \tag{2b}$$

and

$$\kappa=(j+1/2) \quad \text{for} \quad j=l-1/2. \tag{2c}$$

The quantum numbers j and l can be derived from κ according to

$$l=|\kappa+1/2|-1/2 \tag{3}$$

and

$$j=|\kappa|-1/2, \tag{4}$$

i.e., κ specifies uniquely both j and l. The semianalytic expansion of $F(nl_j,Z\alpha)$ about $Z\alpha=0$ for a general atomic state with quantum numbers n, l, and j gives rise to the expression [3]

$$\begin{aligned}F(nl_j,Z\alpha)=&A_{41}(nl_j)\ln[(Z\alpha)^{-2}]+A_{40}(nl_j)\\&+(Z\alpha)A_{50}(nl_j)+(Z\alpha)^2\{A_{62}(nl_j)\ln^2[(Z\alpha)^{-2}]\\&+A_{61}(nl_j)\ln[(Z\alpha)^{-2}]+G_{\mathrm{SE}}(nl_j,Z\alpha)\}.\end{aligned} \tag{5}$$

TABLE IV. A_{60} coefficients for G states.

n	$G_{7/2}$ ($\kappa=4$)	$G_{9/2}$ ($\kappa=-5$)
5	0.000 814 415(1)	0.002 412 929(1)

This expansion is semianalytic, i.e., it involves powers of $Z\alpha$ and of $\ln[(Z\alpha)^{-2}]$. Terms added to the leading order in $Z\alpha$ are commonly referred to as the binding corrections. The coefficients A have two indices, the first of which denotes the power of $Z\alpha$ [including those powers contained in Eq. (1)], while the second index denotes the power of the logarithm $\ln(Z\alpha)^{-2}$.

The limit as $Z\alpha\to 0$ of $G_{\rm SE}(nl_j,Z\alpha)$ is known to be finite and is referred to as the A_{60} coefficient, i.e.,

$$A_{60}(nl_j)=\lim_{Z\alpha\to 0} G_{\rm SE}(nl_j,Z\alpha). \tag{6}$$

Historically, the evaluation of the coefficient A_{60} has been highly problematic. Due to the large number of terms that contribute at relative order $(Z\alpha)^2$ in Eq. (5) and problems concerning the separation of terms that contribute to a specific order in the $Z\alpha$ expansion, evaluations are plagued with severe calculational as well as conceptual difficulties. For example, the evaluation of $A_{60}(1S_{1/2})$ has drawn a lot of attention for a long time [3,11,29–31]. In general, the complexity of the calculation increases with increasing principal quantum number n.

For many states, some of the coefficients in Eq. (5) vanish. Notably, this is the case for P states and for states with higher angular momenta, as a consequence of their behavior at the nucleus, which is less singular than that of S states [specifically, we have $A_{62}(nl_j)=A_{50}(nl_j)=A_{41}(nl_j)=0$ for $l\neq 0$; see Refs. [3,29] and references therein]. The fact that the logarithmic coefficient $A_{71}(nl_j)$ contained in $G_{\rm SE}(nl_j,Z\alpha)$ in Eq. (5) vanishes for $l\neq 0$ has been pointed out in Ref. [32]; it is therefore expected that $A_{7k}(nlj)=0$ for $k>1$. For nonzero l, we thus have

$$F(nl_j,Z\alpha)=A_{40}(nl_j)+(Z\alpha)^2[A_{61}(nl_j)\ln(Z\alpha)^{-2} + A_{60}(nl_j)]+O((Z\alpha)^3) \quad (l\neq 0). \tag{7}$$

For the comparison to experimental data, it is useful to note that the terms in Eqs. (5) and (7) acquire reduced-mass corrections according to Eqs. (2.5a) and (2.5b) of Ref. [33].

The general formula for A_{40} for a non-S state reads (see, e.g., Refs. [2,3,33])

$$A_{40}(nl_j)=-\frac{1}{2\kappa(2l+1)}-\frac{4}{3}\ln k_0(nl), \tag{8}$$

where the Bethe logarithm $\ln k_0(nl)$ is an inherently nonrelativistic quantity, whose expression reads [34] (Sec. 19)

$$\ln k_0(nl)=\frac{n^3}{2(Z\alpha)^4 m}\left\langle \phi\left|\frac{p^i}{m}(H_{\rm S}-E_n) \times\ln\left[2\frac{|H_{\rm S}-E_n|}{(Z\alpha)^2 m}\right]\frac{p^i}{m}\right|\phi\right\rangle. \tag{9}$$

Here, $H_{\rm S}$ is the nonrelativistic Coulomb Hamiltonian $\boldsymbol{p}^2/(2m)-(Z\alpha)/r$, p^i are the components of the momentum operator (i is summed over from 1 to 3), and the ket $|\phi\rangle$ represents the Schrödinger wave function of a state with quantum numbers (n,l), with associated bound-state energy $E_n=-(Z\alpha)^2 m/(2n^2)$. The Bethe logarithm is spin independent and therefore independent of the total angular momentum j for a given orbital angular momentum l; it can be written as a function of n and l alone [factors of Z cancel out in Eq. (9), so that the Bethe logarithm does not depend on Z]. For the atomic levels under investigation here, the Bethe logarithm has been evaluated in Refs. [5,6,35–42] (the results exhibit varying accuracies). Because A_{60} involves relativistic corrections to the coefficient A_{40}, which in turn contains the Bethe logarithm, it is natural to refer to A_{60} as a "relativistic Bethe logarithm."

A general analytic result for the logarithmic correction A_{61} as a function of the bound-state quantum numbers n, l, and j can be inferred from Eq. (4.4a) of Refs. [3,29] upon subtraction of the vacuum-polarization contribution contained in the quoted equation. We have

$$A_{61}(nl_j)=\frac{4}{3}\left\{\frac{8(1-\delta_{l,0})\left(3-\dfrac{l(l+1)}{n^2}\right)}{\prod_{m=-1}^{3}(2l+m)} +\delta_{l,1}\left(1-\frac{1}{n^2}\right)\left(\frac{1}{10}+\frac{1}{4}\delta_{j,l-1/2}\right) +\delta_{l,0}\left[-\frac{601}{240}-\frac{77}{60n^2}+7\ln 2 +3[\gamma-\ln n+\Psi(n+1)]\right]\right\}. \tag{10}$$

Here, Ψ denotes the logarithmic derivative of the Γ function [43] (Sec. 6.3) and γ is Euler's constant [43] (Sec. 6.1.3). We may infer immediately

$$A_{61}(nP_{1/2})=\frac{1}{45}\left(33-\frac{29}{n^2}\right), \tag{11a}$$

$$A_{61}(nP_{3/2})=\frac{2}{45}\left(9-\frac{7}{n^2}\right), \tag{11b}$$

$$A_{61}(nl_j)=\frac{32\left(3-\dfrac{l(l+1)}{n^2}\right)}{3\prod_{m=-1}^{3}(2l+m)} \quad (l\geq 2). \tag{11c}$$

For a given orbital angular momentum l, the coefficient A_{61} approaches a constant as $n\to\infty$. Equation (11c) implies that A_{61} is spin independent for $l\geq 2$, i.e., for D, F, G, . . . states. Therefore, A_{61} does not contribute to the fine structure of these states.

III. THE ϵ METHOD

In this section, we illustrate the usefulness of the so-called ϵ method [11,13,14] in bound-state calculations of QED corrections. It is known that relativistic corrections to the wave function and higher-order terms in the expansion of the bound-electron propagator in powers of Coulomb vertices generate QED corrections of higher order in $Z\alpha$ (see, e.g., Ref. [44] and references therein); these terms manifest themselves in Eq. (5) in the form of the function $G_{\mathrm{SE}}(nl_j,Z\alpha)$, which summarizes these effects at the order of $\alpha(Z\alpha)^6 m$—see Eqs. (1) and (5). It is also well known that for very soft virtual photons, the potential expansion fails and generates an infrared divergence, which is cut off by the atomic momentum scale, $Z\alpha$ (see, e.g., Ref. [44] and references therein). This cutoff for the *infrared* divergence is one of the mechanisms that lead to the logarithmic terms in Eq. (5).

The ϵ method is used for the separation of the two different energy scales for virtual photons: the nonrelativistic domain, in which the virtual photon assumes values of the order of the atomic binding energy, and the relativistic domain, in which the virtual photon assumes values of the order of the electron rest mass. We consider here a model problem with one ''virtual photon,'' which involves the separation of the function being integrated into a high- and a low-energy contribution. This requires the temporary introduction of a parameter ϵ; the dependence on ϵ will cancel at the end of calculation [see Eq. (22) below] when the high- and the low-energy parts are added together. We have

$$\text{nonrelativistic domain} \ll \epsilon \ll \text{electron rest mass},$$

$$\text{i.e., } (Z\alpha)^2 m \ll \epsilon \ll m. \tag{12}$$

The high-energy part is associated with photon energies $\omega > \epsilon$, and the low-energy part is associated with photon energies $\omega < \epsilon$.

In order to illustrate the principles behind the ϵ method, we discuss a simple, one-dimensional example: the evaluation of

$$J(Z\alpha) = \int_0^1 \frac{(Z\alpha)^2-\omega}{(Z\alpha)^2+\omega}\,\frac{1}{\sqrt{1-\omega^2}}\,d\omega, \tag{13}$$

where the integration variable ω may be interpreted as the ''energy'' of a virtual photon. The integral J can be explicitly calculated, so that the perturbation expansion can be checked:

$$J(Z\alpha) = -\frac{\pi}{2} + \frac{2(Z\alpha)^2 \ln\left[\dfrac{1}{(Z\alpha)^2}\left(\sqrt{1-(Z\alpha)^4}+1\right)\right]}{\sqrt{1-(Z\alpha)^4}}. \tag{14}$$

For $|Z\alpha|<1$, this formula is uniquely defined; for other values of $Z\alpha$, the analytic continuations of the logarithm and of the square root have to be performed consistently with the original definition (13).

Within the ϵ method, we start by dividing the calculation of $J(Z\alpha)$ into a high-energy part $J_{\mathrm{H}}(Z\alpha,\epsilon)$ and a low-energy part $J_{\mathrm{L}}(Z\alpha,\epsilon)$, each of which depends on an additional parameter ϵ [that satisfies Eq. (12)]. The sum of the high- and low-energy contributions, which is

$$J(Z\alpha) = J_{\mathrm{H}}(Z\alpha,\epsilon) + J_{\mathrm{L}}(Z\alpha,\epsilon), \tag{15}$$

does not depend on ϵ. Thus, the dependence on ϵ should vanish entirely when we add the high- and low-energy contributions. We may therefore expand both contributions J_{H} and J_{L} first in $Z\alpha$, then in ϵ, and then add them up at the end of the calculation in order to obtain the semianalytic expansion of $J(Z\alpha)$ in powers of $Z\alpha$ and $\ln(Z\alpha)$.

Let us first discuss the ''high-energy part'' of the calculation. It is given by the expression

$$J_{\mathrm{H}}(Z\alpha,\epsilon) = \int_\epsilon^1 \frac{(Z\alpha)^2-\omega}{(Z\alpha)^2+\omega}\,\frac{1}{\sqrt{1-\omega^2}}\,d\omega, \tag{16}$$

where it is important to note in particular the lower integration limit (ϵ). For $\omega > \epsilon$, we may expand

$$\frac{(Z\alpha)^2-\omega}{(Z\alpha)^2+\omega} = -1 + \frac{2(Z\alpha)^2}{\omega} + O((Z\alpha)^4) \tag{17}$$

[see Eq. (12) with $m=1$]. Each corresponding term of Eq. (16) can be integrated, with result

$$J_{\mathrm{H}}(Z\alpha,\epsilon) = \left(-\frac{\pi}{2}+\cdots\right) + 2(Z\alpha)^2\left[\ln\left(\frac{2}{\epsilon}\right)+\cdots\right] + O((Z\alpha)^4), \tag{18}$$

where the ellipsis represents terms that vanish as $\epsilon\to 0$. It is sufficient to only include terms that do not vanish as $\epsilon\to 0$, to each order in $Z\alpha$, because the sum J in Eq. (15) does not depend on ϵ. Moreover, this makes the calculation more manageable. The full cancellation of the dependence on $\ln\epsilon$ will be explicit after we evaluate the ''low-energy part.''

The contribution of the low-energy part ($0<\omega<\epsilon$) reads

$$J_{\mathrm{L}}(Z\alpha,\epsilon) = \int_0^\epsilon \frac{(Z\alpha)^2-\omega}{(Z\alpha)^2+\omega}\,\frac{1}{\sqrt{1-\omega^2}}\,d\omega, \tag{19}$$

where the upper limit of integration depends on ϵ. For $\omega < \epsilon$, we use an expansion that avoids the infrared divergences that we encountered in Eq. (17):

$$\frac{1}{\sqrt{1-\omega^2}} = 1 + \frac{\omega^2}{2} + \frac{3}{8}\omega^4 + \cdots, \tag{20}$$

which leads to a $Z\alpha$ expansion of the low-energy part. We obtain for J_{L}:

$$J_{\mathrm{L}}(Z\alpha,\epsilon) = (\cdots) + 2(Z\alpha)^2\left[\ln\frac{\epsilon}{(Z\alpha)^2}+\cdots\right] + O((Z\alpha)^4\ln^j(Z\alpha)), \tag{21}$$

where the ellipsis again represents terms that vanish as $\epsilon \to 0$, and where j is some integer.

When the high-energy part (18) and the low-energy part (21) are added, the logarithmic divergences in ϵ cancel, as it should, and we have

$$J(Z\alpha) = J_{\mathrm{H}}(Z\alpha,\epsilon) + J_{\mathrm{L}}(Z\alpha,\epsilon)$$
$$= -\frac{\pi}{2} + 2(Z\alpha)^2(\ln[(Z\alpha)^{-2}] + \ln 2)$$
$$+ O((Z\alpha)^4 \ln^j(Z\alpha)) \tag{22}$$

(for some j), which is consistent with Eq. (14). We note the analogy of the above expression with the leading-order terms of the $Z\alpha$ expansion of the function $F(nl_j, Z\alpha)$ given in Eq. (7) for $l \neq 0$ (terms associated to the coefficients A_{40}, A_{61}, and A_{60}). In an actual Lamb shift calculation, the simplifications observed between terms containing ϵ are crucial [13,14].

In this model example, the epsilon method allowed us to obtain Eq. (22) with minimal effort. For comparison, the reader may consider Appendix A of Ref. [45], which illustrates the cancellation of ϵ in higher orders of the $Z\alpha$ expansion, using a different example.

IV. CALCULATION OF SELF-ENERGY COEFFICIENTS

This section, along with the preceding one, gives details of the methods we used in order to obtain the values of the A_{60} coefficient in Tables I–IV (see also Ref. [9]). The purpose of our calculations is to provide data for the self-energy coefficients up to and including the relative order $(Z\alpha)^2$ [see Eq. (7)]; for the states of interest here (non-S states) this corresponds to the coefficients A_{40}, A_{61}, and A_{60}. Equation (8) is the well-known general formula for the coefficient A_{40}. The coefficient A_{61} can be found in Eq. (10), with special cases treated in Eqs. (11a)–(11c). The remaining nonlogarithmic term A_{60} is by far the most difficult to evaluate, and the first results for any state with orbital angular-momentum quantum number $l \geqslant 2$ were recently obtained in Ref. [9] by using the methods described in this section.

As explained in detail in Refs. [11,13,14], the calculation of the one-loop self-energy falls naturally into a high- and a low-energy part (F_H and F_L, respectively). In Sec. III, we illustrated this procedure and the introduction of the scale-separation parameter ϵ for the photon energy. According to Ref. [13] [Eqs. (39)–(43)], the contributions to the low-energy part can be separated naturally into the nonrelativistic dipole and the nonrelativistic quadrupole parts, and into relativistic corrections to the current, to the Hamiltonian, to the binding energy, and to the wave function of the bound state. We follow here the approach outlined in Refs. [13,14], with some modifications.

One main difference as compared to the evaluation scheme described previously concerns the nonrelativistic quadrupole (nq) part. It is given by a specific matrix element [see the definition of P_{nq} in Ref. [13] Eq. (39)], which has to be evaluated for each atomic state and averaged over the angles of the photon wave vectors:

$$\int \frac{d\Omega_k}{4\pi} P_{\mathrm{nq}} = \int \frac{d\Omega_k}{4\pi} \frac{\delta^{\mathrm{T},ij}}{6m}$$
$$\times \left[\left\langle \phi \middle| p^i e^{i\boldsymbol{k}\cdot\boldsymbol{r}} \frac{1}{H_S - (E-\omega)} p^j e^{-i\boldsymbol{k}\cdot\boldsymbol{r}} \middle| \phi \right\rangle \right.$$
$$\left. - \left\langle \phi \middle| p^i \frac{1}{H_S - (E-\omega)} p^j \middle| \phi \right\rangle \right], \tag{23}$$

where the transverse δ function is given by

$$\delta^{\mathrm{T},ij} = \delta^{ij} - \frac{k^i k^j}{\boldsymbol{k}^2}.$$

The dipole interaction obtained by the replacement

$$\exp(i\boldsymbol{k}\cdot\boldsymbol{r}) \to 1$$

is subtracted; it leads to a lower-order contribution. The next term in the Taylor expansion of the exponential reads

$$\int \frac{d\Omega_k}{4\pi} \frac{\delta^{\mathrm{T},ij}}{6m} \left[\left\langle \phi \middle| p^i (\boldsymbol{k}\cdot\boldsymbol{r}) \frac{1}{H_S - (E-\omega)} p^j (\boldsymbol{k}\cdot\boldsymbol{r}) \middle| \phi \right\rangle \right.$$
$$\left. - \left\langle \phi \middle| p^i \frac{1}{H_S - (E-\omega)} p^j (\boldsymbol{k}\cdot\boldsymbol{r})^2 \middle| \phi \right\rangle \right]. \tag{24}$$

This representation makes an evaluation in coordinate space possible. However, an evaluation of this expression leads to a rather involved angular-momentum algebra. Specifically, we employ a well-known angular-momentum decomposition of the coordinate-space hydrogen Green function [46]

$$G(\boldsymbol{r}_1, \boldsymbol{r}_2, E-\omega) = \sum_{l',m} g_{l'}(r_1, r_2, \nu) Y_{l',m}(\hat{\boldsymbol{r}}_1) Y^*_{l',m}(\hat{\boldsymbol{r}}_2), \tag{25}$$

with $E - \omega = -\alpha^2 m/(2\nu^2)$ and [47]

$$g_{l'}(r_1, r_2, \nu) = \frac{4m}{a\nu} \left(\frac{2r_1}{a\nu}\right)^{l'} \left(\frac{2r_2}{a\nu}\right)^{l'} e^{-(r_1+r_2)/(a\nu)}$$
$$\times \sum_{k=0}^{\infty} \frac{L_k^{2l'+1}\left(\frac{2r_1}{a\nu}\right) L_k^{2l'+1}\left(\frac{2r_2}{a\nu}\right)}{(k+1)_{2l'+1}(l'+1+k-\nu)}, \tag{26}$$

where $a = 1/(Z\alpha m)$, $(k)_c$ is the Pochhammer symbol, and L denotes associated Laguerre polynomials [43]. For a reference state $|\phi\rangle$ of orbital angular momentum l, we obtain in Eq. (24) nonzero contributions from Green-function components (25) with $l' = l-2, l-1, l, l+1, l+2$. They can be obtained by a straightforward, but tedious, application of angular-momentum algebra (see, e.g., Ref. [48]).

As in previous calculations [see also Ref. [13] [Eqs. (18) and (19)] and [14] [Eqs. (55)–(58)]], we obtain for the high-energy part of all atomic states the general structure

$$F_H(nl_j,Z\alpha)=-\frac{1}{2\kappa(2l+1)}+(Z\alpha)^2 \times\left[\mathcal{K}-\frac{\mathcal{C}}{\epsilon}-A_{61}\ln(2\epsilon)+O(\epsilon)\right]+\cdots, \tag{27}$$

where $\mathcal{K}$ is a constant and the ellipsis denotes higher-order terms [in $Z\alpha$ and $\ln(Z\alpha)$]. As observed in Sec. III, we may suppress terms that vanish in the limit $\epsilon\to O$ [terms of the form $O(\epsilon)$ in the $(Z\alpha)^2$ term in Eq. (27) above]. These terms cancel when the high- and low-energy parts are added.

Together with the constant term $-A_{61}\ln 2$, the constant $\mathcal{K}$ contributes to A_{60}. $\mathcal{C}$ is the coefficient of the $1/\epsilon$ divergence; the term $-\mathcal{C}/\epsilon$ cancels when the high- and low-energy parts are added. Both $\mathcal{K}$ and $\mathcal{C}$ are state dependent and vary with n,j,l. As in Refs. [13] [Eqs. (56) and (57)] and [14] [Eqs. (89)–(92)], the low-energy part, for all states under investigation, has the general structure

$$F_L(nl_j,Z\alpha)=-\frac{4}{3}\ln k_0(nl) +(Z\alpha)^2\left[\mathcal{L}+\frac{\mathcal{C}}{\epsilon}+A_{61}\ln\left(\frac{\epsilon}{(Z\alpha)^2}\right)+O(\epsilon)\right] +\cdots, \tag{28}$$

where $\ln k_0(nl)$ is the Bethe logarithm [see Eq. (9)] and the ellipsis denotes higher-order terms. The cancellation of the divergence in ϵ between Eqs. (27) and (28) is obvious. The constant $\mathcal{L}$, which is state dependent (a function of n,j,l), represents the low-energy contribution to A_{60} and can be interpreted as the relativistic generalization of the Bethe logarithm. In terms of the general expressions (27) and (28), A_{60} is therefore given by

$$A_{60}=\mathcal{K}-A_{61}\ln 2+\mathcal{L}. \tag{29}$$

Our improved results for A_{60} coefficients rely essentially on a more general code for the analytic calculations, written in the computer-algebra package MATHEMATICA [49,50], which enables the corrections to be evaluated semiautomatically. Intermediate expressions with some 200 000 terms are encountered, and the complexity of the calculations sharply increases with the principal quantum number n and, as far as the complexity of the angular-momentum algebra is concerned, with the orbital angular quantum number of the bound electron.

Of crucial importance was the development of convergence acceleration methods which were used extensively for the evaluation of remaining one-dimensional integrals, which could not be done analytically. These integrals are analogous to expressions encountered in previous work [see Eqs. (36), (47), and (48) of Ref. [13] and Eqs. (80)–(84) of Ref. [14]]. The numerically evaluated contributions involve slowly convergent hypergeometric series and, in more extreme cases, infinite series over partial derivatives of hypergeometric functions, and generalizations of Lerch's Φ transcendent [51,52]. As a result of the summation over l' in Eq. (25), after performing radial integrals, two specific hypergeometric functions enter naturally into the expressions for the bound-state matrix elements that characterize the one-loop correction [see, e.g., Eqs. (80) and (81) of Ref. [14]]. One of these functions is given by

$$\Phi_1(n,t)={}_2F_1\left(1,-nt,1-nt,\left(\frac{1-t}{1+t}\right)^2\right), \tag{30}$$

where the integration variable t is in the range 0–1 and n is the bound-state principal quantum number (${}_2F_1$ denotes the hypergeometric function—see, e.g., Chap. 15 in Ref. [43]). For $t\simeq 0$, the power-series expansion of Φ_1 is slowly convergent,

$$\Phi_1(n,t)=(nt)\sum_{k=0}^{\infty}\frac{\left(\frac{1-t}{1+t}\right)^{2k}}{nt-k}. \tag{31}$$

The series is nonalternating. In order to accelerate the convergence in the range $t\in(0,0.05)$, we employ the combined nonlinear-condensation transformation [7,28]. The other hypergeometric function that occurs naturally in our calculations is

$$\Phi_2(n,t)={}_2F_1\left(1,-nt,1-nt,-\left(\frac{1-t}{1+t}\right)\right). \tag{32}$$

For $0<t<0.05$, we accelerate the convergence of the alternating power series

$$\Phi_2(n,t)=(nt)\sum_{k=0}^{\infty}\frac{\left(-\frac{1-t}{1+t}\right)^{k}}{nt-k} \tag{33}$$

via the δ transformation [53] [Eq. (8.4-4)]. The convergence acceleration leads to a much more reliable evaluation of the remaining numerical integrals which contribute to A_{60} (but cannot be expressed in closed analytic form). As a by-product of our investigations, we obtained through this (independent) method Bethe logarithms which are consistent with the precise results of Ref. [5]. Here, we restrict the accuracy to 24 figures and give results for P states:

$$\begin{aligned}
\ln k_0(2P)&=-0.030\,016\,708\,630\,212\,902\,443\,676(1),\\
\ln k_0(3P)&=-0.038\,190\,229\,385\,312\,447\,701\,163(1),\\
\ln k_0(4P)&=-0.041\,954\,894\,598\,085\,548\,671\,037(1),\\
\ln k_0(5P)&=-0.044\,034\,695\,591\,877\,795\,070\,318(1).
\end{aligned} \tag{34}$$

These results, which test the numerical methods that we employed, are in agreement with other recent calculations [5,6,41,42].

The main results of this paper concerning the A_{60} coefficients are given in Tables I–IV, with an absolute precision of 10^{-9}. In addition, we give explicit expressions for the low- and high-energy parts of the self-energy, for the states with

TABLE V. According to Eqs. (27) and (28), the high- and low-energy parts can be cast into a general form involving the terms $\mathcal{C}$, $\mathcal{K}$, and $\mathcal{L}$. The coefficient A_{60} can be expressed in terms of $\mathcal{K}$, A_{61}, and $\mathcal{L}$ according to Eq. (29). Here, we present analytic results for the terms $\mathcal{C}$, A_{61}, and $\mathcal{K}$, and numerical results for $\mathcal{L}$ (for states with $n=5$). The results for A_{61} can be inferred from Eqs. (10)–(11c). For $l \geqslant 2$, we observe that A_{61} are spin independent and that $\mathcal{C}=A_{61}$.

$\mathcal{C}$, $\mathcal{K}$, and $\mathcal{L}$ coefficients for states with $n=5$				
State	$\mathcal{C}$	A_{61}	$\mathcal{K}$	$\mathcal{L}$
$5P_{1/2}$	$\frac{292}{1125}$	$\frac{796}{1125}$	$\frac{20129}{67500}$	$-1.023\,991\,781(1)$
$5P_{3/2}$	$\frac{292}{1125}$	$\frac{436}{1125}$	$\frac{199387}{540000}$	$-0.747\,615\,653(1)$
$5D_{3/2}$	$\frac{92}{7875}$	$\frac{92}{7875}$	$-\frac{35947}{3780000}$	$0.023\,759\,683(1)$
$5D_{5/2}$	$\frac{92}{7875}$	$\frac{92}{7875}$	$\frac{3097}{157500}$	$0.021\,511\,798(1)$
$5F_{5/2}$	$\frac{2}{1125}$	$\frac{2}{1125}$	$-\frac{2657}{1102500}$	$0.006\,045\,397(1)$
$5F_{7/2}$	$\frac{2}{1125}$	$\frac{2}{1125}$	$\frac{774121}{211680000}$	$0.005\,662\,248(1)$
$5G_{7/2}$	$\frac{2}{4725}$	$\frac{2}{4725}$	$-\frac{4397}{6048000}$	$0.001\,834\,827(1)$
$5G_{9/2}$	$\frac{2}{4725}$	$\frac{2}{4725}$	$\frac{269}{283500}$	$0.001\,757\,471(1)$

$n=5$ under investigation [see Eqs. (27) and (28) and Table V]. They may be helpful in an independent verification of our calculations. Note that the $G_{7/2}$ and $G_{9/2}$ states involve the most problematic angular-momentum algebra of all atomic states considered here.

For some P states (see Table I), the values of A_{60} reported here are four orders of magnitude more accurate than previous results [13,14], due to the improved numerical algorithms. For the $3P_{1/2}$ state, the numerical value for the A_{60} coefficient of Table I differs from the previously reported result [14] by more than the numerical uncertainty quoted in Ref. [14], whereas agreement with previous results [13,14] is obtained in the case of $2P_{1/2}$ and $4P_{1/2}$ states. The discrepancy for $A_{60}(3P_{1/2})$ is on the level of 5×10^{-4} in absolute units, which corresponds to roughly 2 Hz (in frequency units) on the self-energy correction in atomic hydrogen. The computational error in Ref. [14] was caused by numerical difficulties in one of the remaining one-dimensional integrals involving the hypergeometric functions (30) and (32), which could not be evaluated analytically. The numerical difficulties encountered in previous calculations due to slow convergence of the integrals are essentially removed by the convergence acceleration techniques.

For some states, rather severe numerical cancellations are observed between the high- and low-energy contributions to the self-energy, as well as between the different contributions to the low-energy part. This intriguing observation is documented in Tables VI and VII, using the $5G_{7/2}$ state as an example. Note that these numerical cancellations go beyond the required exact, analytic cancellation of the divergent contributions which depend on the scale-separation parameter ϵ.

V. A_{60} FOR HIGHER-n STATES

This section contains approximate formulas for the A_{60} coefficients of P and D states, for principal quantum numbers n, which go beyond those of Tables I and II. These

TABLE VI. As explained in Refs. [13,14], the low-energy contributions to A_{60} naturally separate into the following terms: the nonrelativistic quadrupole part $F_{\rm nq}$ [13] [Eq. (39)], the relativistic corrections to the current $F_{\delta y}$ [13], [Eq. (40)], relativistic corrections to the Hamiltonian $F_{\delta \rm H}$ [13] [Eq. (41)], and relativistic corrections to the bound-state energy $F_{\delta \rm E}$ [13] [Eq. (42)] and to the wave function $F_{\delta\phi}$ [13] [Eq. (43)]. This classification suggests that it is natural to refer to the low-energy contribution $\mathcal{L}$ as a relativistic Bethe logarithm. The total contribution to A_{60} of the low-energy part, which reads $0.001\,834\,827(1)$, is roughly five times smaller than the largest individual contribution (from $F_{\delta \rm H}$), due to cancellations.

Contributions to the low-energy part ($5G_{7/2}$)	
A_{60} contribution due to $F_{\rm nq}$	$0.002\,875\,830\,9(5)$
A_{60} contribution due to $F_{\delta y}$	$-0.001\,083\,109\,4(5)$
A_{60} contribution due to $F_{\delta \rm H}$	$-0.008\,917\,782\,1(5)$
A_{60} contribution due to $F_{\delta \rm E}$	$0.004\,920\,556\,0(5)$
A_{60} contribution due to $F_{\delta\phi}$	$0.004\,039\,332\,1(5)$
A_{60} (see entry for $\mathcal{L}$ in Table V)	$0.001\,834\,827(1)$

tables contain enough values of $A_{60}(nl_j)$ for extrapolations to be made. We represent the asymptotic behavior of $A_{60}(nl_j)$ as $n\to\infty$ as

$$A_{60}(nl_j)=\mathcal{A}_3(n,l_j)+O\left(\frac{1}{n^3}\right), \tag{35a}$$

where

$$\mathcal{A}_3(n,l_j)=a_0(l_j)+\frac{a_1(l_j)}{n}+\frac{a_2(l_j)}{n^2}. \tag{35b}$$

Such an asymptotic behavior is motivated, for any non-S state, by its similarity to the functional form of the self-energy coefficient A_{61} in Eq. (7)—see Eq. (11). The values that we obtained for the coefficients $a_i(l_j)$ can be found in Table VIII. The fitting method is described in the Appendix.

The approximation $\mathcal{A}_3(n,l_j)$ to $A_{60}(nl_j)$ is depicted in Fig. 1, for P and D states. According to the graphs in this figure, the $O(1/n^3)$ contribution in Eq. (35a) is much smaller than the uncertainty in $\mathcal{A}_3$, which comes from the uncertainties in the coefficients of Table VIII.

The coefficients a_i of Eq. (35b) given in Table VIII can be useful to spectroscopy experiments that involve electronic levels with principal quantum numbers that are higher than

TABLE VII. For the $5G_{7/2}$ state, an additional numerical cancellation occurs when the finite contributions to A_{60} originating from the low-energy part (see the ninth row of Table V) and the high-energy part are added according to Eq. (29). The high-energy contribution is $A_{60}(F_{\rm H})=\mathcal{K}-A_{61}\ln 2$, and the low-energy contribution is $A_{60}(F_{\rm L})=\mathcal{L}$.

$A_{60}(F_{\rm H})$	$-0.001\,020\,413$
$A_{60}(F_{\rm L})$	$0.001\,834\,828(1)$
A_{60}	$0.000\,814\,415(1)$

TABLE VIII. The asymptotic behavior of $A_{60}(nl_j)$ as $n\to\infty$ can be described by an expansion in $1/n$. The following table contains the first coefficients of such an expansion, as defined in Eq. (35). The approximate values of $A_{60}(nl_j)$ that can be directly deduced from this table and from Eq. (35b) are the best available values of A_{60} for P and D states, except for the states that are represented in Tables I and II. These results are depicted in Fig. 1.

State	a_0	a_1	a_2
$P_{1/2}$	−1.249(9)	0.0(2)	0.87(45)
$P_{3/2}$	−0.69(2)	0.15(5)	0.25(25)
$D_{3/2}$	0.011(1)	−0.032(7)	−0.05(9)
$D_{5/2}$	0.034(2)	0.025(5)	−0.18(4)

those of Tables I and II. In fact, the self-energy of the electron of a hydrogenlike ion can be estimated through Eqs. (7), (8), (11), and (35), with $\mathcal{A}_3$ defined with the values of Table VIII. Hydrogen has been and will be the subject of extremely precise spectroscopy experiments, which now approach the level of 1 Hz of uncertainty in transition frequencies. The uncertainty in the self-energy (1) which comes from the uncertainties in the coefficients of Table VIII through Eqs. (7) and (35) is comparable to the current experimental limit. In fact, the uncertainties in $\mathcal{A}_3$ in Eq. (35b) contribute to the self-energy less than ± 2 Hz for $P_{1/2}$ states with $n>7$, less than ± 1.6 Hz for $P_{3/2}$ states with $n>7$, less than ± 0.12 Hz for $D_{3/2}$ states with $n>8$, and less than ± 0.12 Hz for $D_{5/2}$ states with $n>8$ (precise values of A_{60} for lower values of n can be found in Tables I and II).

Moreover, the coefficients of Table VIII can be useful for theoretical calculations. In fact, future values of A_{60} for P and D states can be checked against the estimates provided by $\mathcal{A}_3$ in Eq. (35b)—see also the curves of Fig. 1.

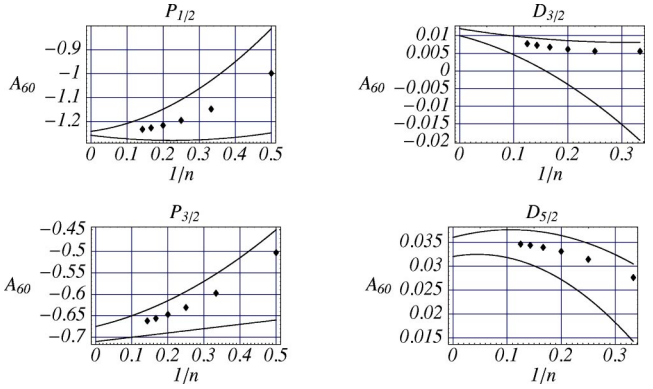

FIG. 1. These graphs show exact and approximate values of the self-energy coefficient A_{60}—see Eq. (7). Exact values are represented by dots and can be found in Tables I and II. The two curves of each graph represent the upper and lower limits of the approximation to A_{60} provided by $\mathcal{A}_3$ in Eqs. (35), by taking into account the uncertainties in the coefficients of Table VIII. For levels in hydrogen with principal quantum number $n\geqslant 10$, the uncertainty in A_{60} deduced from these curves contributes to the uncertainty in the electron self-energy (1) by less than 2 Hz. (The use of $1/n$ as the abscissa allows all large principal quantum numbers n to be represented in the graphs.)

VI. APPROXIMATIONS FOR A_{60} AND FOR THE BETHE LOGARITHM

In addition to studying the dependence of $A_{60}(nl_j)$ on n, as we did in the preceding section for P and D states, it is interesting to analyze the behavior of $A_{60}(nl_j)$ as a function of l, for $j=l-1/2$ and $j=l+1/2$. We conjecture that $A_{60}(\overline{nl}_j)$, for $\overline{n}=l+1$ and $j=l\pm 1/2$, decreases as

$$A_{60}(\overline{nl}_j) \overset{l\to\infty}{\sim} \frac{c(j-l)}{l^k} \text{ with } k\geqslant 3, \tag{36}$$

where we probably have $k=4$ or $k=5$ [$c(1/2)$ and $c(-1/2)$ are two unspecified numbers]. Form (36) is motivated in this section.

We have also studied the asymptotic behavior of the Bethe logarithm $\ln k_0(\overline{nl})$ because this is a quantity similar to the "relativistic Bethe logarithm" A_{60} and it yields a large contribution to the self-energy [see Eqs. (7) and (8)]. We show in this section that the Bethe logarithm $\ln k_0(\overline{nl})$, where $\overline{n}=l+1$, appears to behave asymptotically as l^{-3}. This result differs from the $l^{-7/2}$ asymptotic behavior of $\ln k_0(\overline{nl})$ deduced from Eq. (B5) in Ref. [54] (p. 845). Extrapolations of the Bethe logarithm $\ln k_0(nl)$ as a function of n have been obtained through the method described in the Appendix, and used in Ref. [55] for S, P, and D states ($l=0$–2).

We also postulate that the Bethe logarithm $\ln k_0(\overline{nl})$, where $\overline{n}=l+1$, can be expanded in powers of l^{-1} about $l=\infty$. In order to find the first five coefficients of such an expansion, we used the fitting procedure described in the Appendix. The resulting approximation reads

$$l^3 \ln k_0(\overline{nl}) \simeq \left(-0.056\,853(2) + \frac{0.024\,78(4)}{l} + \frac{0.0387(8)}{l^2} + \frac{-0.114(6)}{l^3} + \frac{0.16(2)}{l^4} \right), \tag{37}$$

where $\overline{n}=l+1$ and the neglected contribution is of order l^{-5}. This approximation should be valid for $l\to\infty$; nevertheless, it yields values of the Bethe logarithm that are both precise (see Fig. 2) and compatible with all the values of $\ln k_0(\overline{nl})$ for $l=3,\ldots,19$ (taken from Ref. [6]). For the $l\geqslant 20$ levels of hydrogen, the uncertainty in the result of approximation (37) is negligible, when compared to the best experimental uncertainty in transition frequency measurements (about 1 Hz [1]).

Moreover, we suggest that the orders of magnitude of the self-energy coefficient $A_{60}(nl_j)$ and of the Bethe logarithm $\ln k_0(nl)$ do not depend on the principal quantum number n, i.e., the order of magnitude of a coefficient $A_{60}(nl_j)$ is given by the order of magnitude of $A_{60}(\overline{nl}_j)$, where $\overline{n}=l+1$ (and similarly for the Bethe logarithm). For A_{60}, this behavior is a generalization of what is observed for P, D, F, and G states in Tables I–IV. For the Bethe logarithm, the fact that

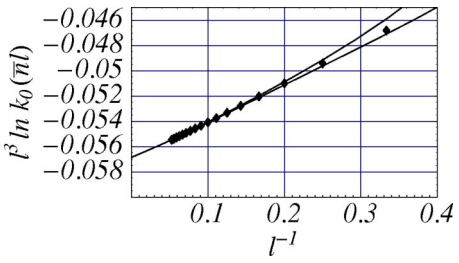

FIG. 2. Comparison between exact values of $l^3 \ln k_0(\overline{nl})$ (dots) and the truncated asymptotic expansion of Eq. (37) (where the upper and lower limits are represnted by the two curves), where $\ln k_0(\overline{nl})$ is the Bethe logarithm, and $\overline{n}=l+1$. The numerical values of the Bethe logarithms used in this graph [6] are compatible with the values deduced from Eq. (37), which are in the area between the two curves. The fact that the data points seem to converge toward a finite value ($\simeq -0.057$) as $l^{-1}\to 0$ supports the conjecture of an l^{-3} asymptotic behavior of the Bethe logarithm $\ln k_0(\overline{nl})$.

$\ln k_0(nl)$ and $\ln k_0(\overline{nl})$ have the same order of magnitude can be observed for states with $l<n\leqslant 20$ by inspecting the results of Ref. [6].

The expressions (36) and (37) for the asymptotic behavior of $A_{60}(\overline{nl}_j)$ and $\ln k_0(\overline{nl})$, where $\overline{n}=l+1$, could thus be used for estimating the order of magnitude of the self-energy with the help of Eqs. (7), (8), and (11). Estimating the self-energy correction (1) can be useful in high-precision spectroscopy experiments with large-l levels. Thus, for instance, a recent experiment [8] required evaluating the self-energies of circular ($n=l+1$) states of orbital quantum number $l\simeq 30$. On the theoretical side, future calculations of $A_{60}(nl_j)$ and $\ln k_0(nl)$ can be checked against the asymptotic behaviors of $A_{60}(\overline{nl}_j)$ and $\ln k_0(\overline{nl})$ which are described above.

Since the order of magnitude of $A_{60}(nl_j)$ does not appear to depend on n, it is natural to represent it (for fixed l and j) by the order of magnitude of either $\lim_{n\to\infty} A_{60}(nl_j)$—largest possible n— or $A_{60}(\overline{nl}_j)$, where $\overline{n}=l+1$ is the smallest n possible for the angular-momentum quantum number l. We chose the latter possibility for two reasons. First, small-n values of $A_{60}(nl_j)$ are available (see Tables I–IV). Second, future values of $A_{60}(nl_j)$ for higher angular quantum numbers l are likely to be obtained first for states where $n=l+1$, which is the smallest n possible for a given angular-momentum quantum number l. In particular, such states have simpler radial wave functions (the number of terms in the radial wave function of a state increases with $n-l$). And finally, circular states ($n=l+1$) are relevant to high-precision spectroscopy experiments (see, e.g., Ref. [8]), whereas $n=\infty$ states are unphysical.

As mentioned above, we expect an asymptotic behavior of the form l^{-k}, with k integer, for $A_{60}(\overline{nl}_j)$ and for the Bethe logarithm $\ln k_0(\overline{nl})$. Such a functional form is motivated by the fact that all the $A_{ik}(nl_j)$ coefficients of the self-energy function F in Eq. (5) can be expanded in power series of $1/n$ and l^{-1}, except maybe for the two coefficients related to this section, A_{60} and A_{40}, where the latter is a function of the Bethe logarithm [see Eq. (8)]. (We suppose that A_{60} and A_{40} can also be expanded in such a series.) This

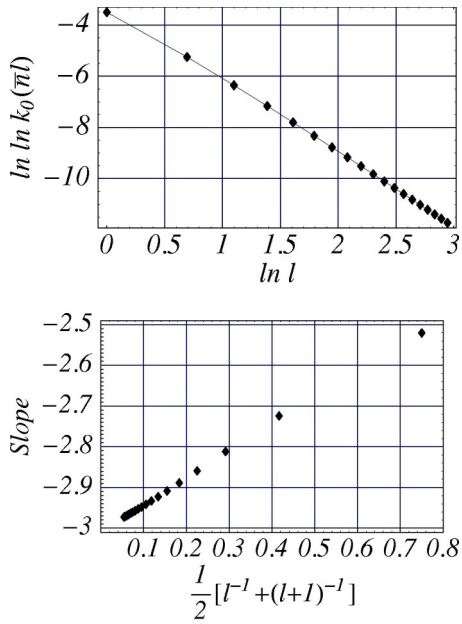

FIG. 3. Upper graph: log-log plot of the Bethe logarithm $\ln k_0(\overline{nl})$, where $\overline{n}=l+1$. Lower graph: slope between two successive points of the log-log plot. The limit slope of -3 as $l\to\infty$ observed in the lower graph indicates that the Bethe logarithm $\ln k_0(\overline{nl})$ behaves asymptotically as l^{-3}. This confirms what is observed in Fig. 2. (The abscissa of the points in the lower graph is chosen so as to produce a graph from which the limit slope of the upper graph as $l\to\infty$ can be easily deduced.)

can, for instance, be checked with the formulas for $A_{ik}(nl_j)$ reviewed in Ref. [2] (p. 468) with the help of Eq. (10) for $A_{61}(nl_j)$, where $\Psi(n+1)$ can be expanded in powers of $1/(n+1)$ [43] (Sec. 6.3.18).

The l^{-3} behavior of the Bethe logarithm $\ln k_0(\overline{nl})$, where $\overline{n}=l+1$, is suggested by Fig. 2. The points of this graph, which represent

$$l^3 \ln k_0(\overline{nl}), \tag{38}$$

appear to converge toward a limit ($\simeq -0.057$) as $l^{-1}\to 0$. We checked the l^{-3} behavior deduced from the study of Eq. (38) by calculating the slope of a log-log plot of the Bethe logarithm $\ln k_0(\overline{nl})$ (with numerical values taken from Ref. [6]). The result, shown in Fig. 3, indicates that the Bethe logarithm does indeed behave asymptotically as l^{-3}; this coincides with the conclusion from Fig. 2.

It is possible to use the procedure depicted in Fig. 3 to estimate the integer exponent k of an asymptotic behavior l^{-k} for the *relativistic* Bethe logarithm $A_{60}(\overline{nl}_j)$, where $\overline{n}=l+1$ and $j=l\pm 1/2$. In fact, it is reasonable to use the Bethe logarithm $\ln k_0(\overline{nl})$ as a guide for studying the *relativistic* Bethe logarithm A_{60}. Thus, the procedure depicted in Fig. 3 was applied to the self-energy coefficient $A_{60}(\overline{nl}_j)$; we obtained the asymptotic behavior presented at the beginning of this section, and in particular in Eq. (36). The graphs supporting Eq. (36) are given in Fig. 4 for states with $j=l+1/2$, and in Fig. 5 for states with $j=l-1/2$. Each of these

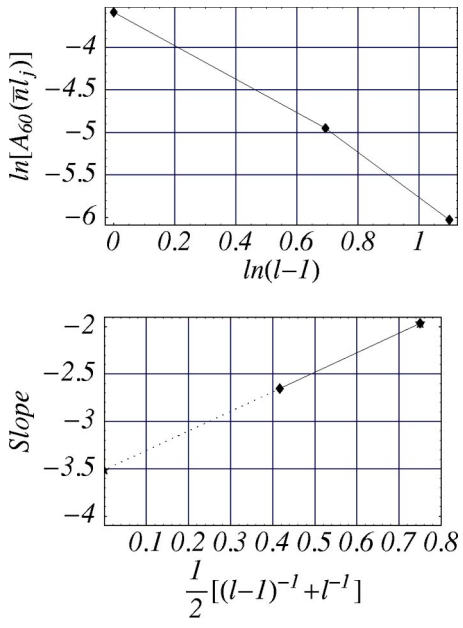

FIG. 4. Upper graph: log-log plot of the self-energy coefficient $A_{60}(\overline{nl}_j)$, where $\overline{n}=l+1$ and $j=l+1/2$. Lower graph: slope between two successive points of the log-log plot (solid line) and extrapolation to $l\to\infty$ (dashes). By analogy with the graphs similarly obtained for the Bethe logarithm in Fig. 3, we conclude that for $j=l+1/2$, $A_{60}(\overline{nl}_j)$ behaves asymptotically as l^{-k} with $k\geqslant 3$ and, probably, $k=4$ or $k=5$. The values of A_{60} are taken from Tables II–IV.

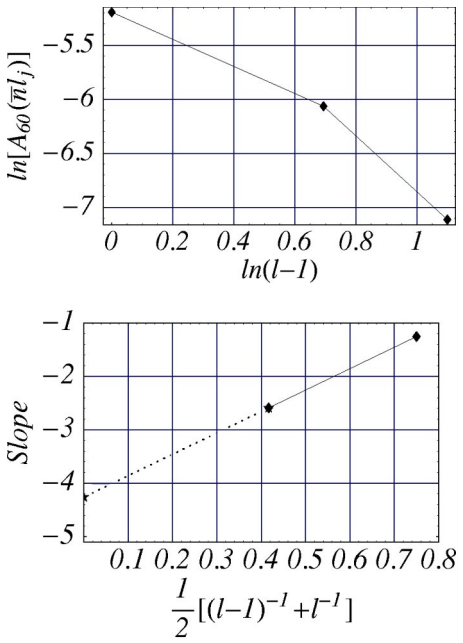

FIG. 5. Upper graph: log-log plot of the self-energy coefficient $A_{60}(\overline{nl}_j)$, where $\overline{n}=l+1$ and $j=l-1/2$. Lower graph: slope between two successive points of the log-log plot (solid line) and extrapolation to $l\to\infty$ (dashes). By analogy with the graphs similarly obtained for the Bethe logarithm in Fig. 3, we conclude that for $j=l-1/2$, $A_{60}(\overline{nl}_j)$ behaves asymptotically as l^{-k} with $k\geqslant 3$ and, probably, $k=4$ or $k=5$. The values of A_{60} are taken from Tables II–IV.

graphs uses only three values of A_{60} (D, F, and G states); even though this is a relatively small number of values compared to the number of available values of the Bethe logarithm, the behavior of the first few data points in Fig. 3 justifies using only a few small-l values in order to predict the asymptotic behavior of $A_{60}(\overline{nl}_j)$ for $l\to\infty$.

The values of the A_{60} coefficient of S and P states were not used in obtaining Eq. (36), because it is convenient to treat the orders of magnitude of the A_{60} coefficient of these states separately from the orders of magnitude of higher-l states; Fig. 6 illustrates this point. We note that the self-energy coefficient A_{61} also exhibits an exceptional behavior for S and P states [see, e.g., Eq. (4.4a) in Ref. [3]]. As an additional consequence, estimating the coefficient c of the asymptotic form of A_{60} in Eq. (36) would require the use of states with orbital angular-momentum quantum number $l\geqslant 2$ (D, F, etc.).

The possible values of the exponent k in Eq. (36) deduced from both the graphs of Figs. 4 and 5 are compatible with each other ($k\geqslant 3$ with, probably, $k=4$ or $k=5$). It is indeed expected that the asymptotic form of $A_{60}(\overline{nl}_j)$ be the same for $j=l+1/2$ and $j=l-1/2$, as can be seen from the numerical values for D, F, and G states found in Tables II–IV. More precise estimates of the asymptotic exponent k in Eq. (36) can be obtained through the procedure we used in Figs. 4 and 5, as soon as additional values of $A_{60}(\overline{nl}_j)$ with $\overline{n}=l+1$ are available.

According to the results of this section, the "*relativistic* Bethe logarithm" $A_{60}(\overline{nl}_j)$ decreases at least as fast (and probably one or two powers faster), as a function of l, as the Bethe logarithm $\ln k_0(\overline{nl})$. Such a behavior is also found in the (Dirac-Coulomb) energy of hydrogen and hydrogenlike ions. Thus, the Dirac-Coulomb energy of an electron bound to a nucleus of charge number Z is [see, e.g., [2], p. 466]

$$E_{nj}=\left[1+\frac{(Z\alpha)^2}{(n-\delta)^2}\right]^{-1/2}, \tag{39}$$

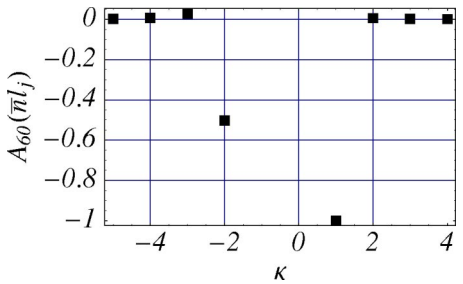

FIG. 6. This graph shows values of the self-energy coefficients $A_{60}(\overline{nl}_j)$, where $\overline{n}=l+1$, as a function of the Dirac quantum number κ, where κ is defined in Eq. (2). The large value $A_{60}(1S_{1/2})\simeq -31$ is not represented here. This plot shows that for S and P states ($\kappa=-2$, -1, and 1), the A_{60} coefficient exhibits an exceptional behavior; such an exceptional behavior is also found in the self-energy coefficient A_{61} in Eq. (10), which is known analytically.

where

$$\delta=(j+1/2)-\sqrt{(j+1/2)^2-(Z\alpha)^2}.$$

According to Eq. (39), an electron in a circular state $\overline{nl}_j$ with $j=l+1/2$ (and $\overline{n}=l+1$) has an energy

$$E^{-}_{n,l+(1/2)}=\sqrt{1-[Z\alpha/(l+1)]^2}. \tag{40}$$

In the Taylor expansion (in $Z\alpha$) of this energy, the asymptotic behavior of the coefficient of $(Z\alpha)^{2k}$ is given by l^{-2k} (this conclusion also holds for circular state $\overline{nl}_j$ with $j=l-1/2$). Thus, for circular states, successive relativistic corrections to the nonrelativistic energy of a bound electron fall off faster and faster with the orbital quantum number l, with two additional powers of l^{-1} for each order in $(Z\alpha)^2$. If this rule applies to the coefficients of the self-energy expansion (7), the asymptotic form of $A_{60}(\overline{nl}_j)$ as $l\to\infty$ should be l^{-4}; in fact, the lower-order coefficient $A_{40}(\overline{nl}_j)$ decreases as l^{-2}, as can be seen in Eq. (8). On the other hand, since $A_{60}(nl_j)$ can be viewed as a relativistic correction to the Bethe logarithm, applying the above rule yields an asymptotic form in l^{-5} for $A_{60}(\overline{nl}_j)$, since the Bethe logarithm behaves as l^{-3}, as described in this section. These observations are fully compatible with the graphs of Figs. 4 and 5, from which the asymptotic form (36) of $A_{60}(\overline{nl}_j)$ was deduced (with an exponent k probably equal to 4 or 5).

VII. CHECKS OF THE A_{60} COEFFICIENTS

We have checked our analytic results for A_{60} (cf. Tables I–IV) by an independent method: the analytic results were compared to values deduced from nonperturbative, numerical calculations of the self energy (1). We have used the numerical self-energy values of Refs. [15,23,27,56–58], as well as new values [59], which extend the results of Ref. [27] to smaller nuclear charge numbers Z (to Z between 10 and 25). In most cases, the checks that we detail below *confirm* the values of A_{60} reported in Tables I–IV to a relative precision of about 15%. The few exceptions are the following. For $2P$ states, the numerical values of the self-energy confirm the results of Table I to about 1%. For $nD_{3/2}$ states with $n=3,\ldots,8$, the nonperturbative self-energy results yield $A_{60}(nD_{3/2})=0.005(10)$, in agreement with the results of Table II. And finally, we did not check $A_{60}(8D_{5/2})$ in Table II by using nonperturbative self-energy values because no such values are available for the $8D_{5/2}$ state. However, as depicted in Fig. 1, the value of $A_{60}(8D_{5/2})$ reported here appears to fit well within the series of $A_{60}(nD_{5/2})$ values for $n=3,\ldots,7$ (see Table II).

The first check that we applied consisted of comparing the numerical, exact results for F to two of its successive approximations. The first approximation, $F^{(2)}(Z\alpha)$, includes the *two* dominant and already-known coefficients A_{40} (8) and A_{61} (10) of expansion (7):

$$F^{(2)}(Z\alpha)=A_{40}+(Z\alpha)^2A_{61}\ln(Z\alpha)^{-2}, \tag{41}$$

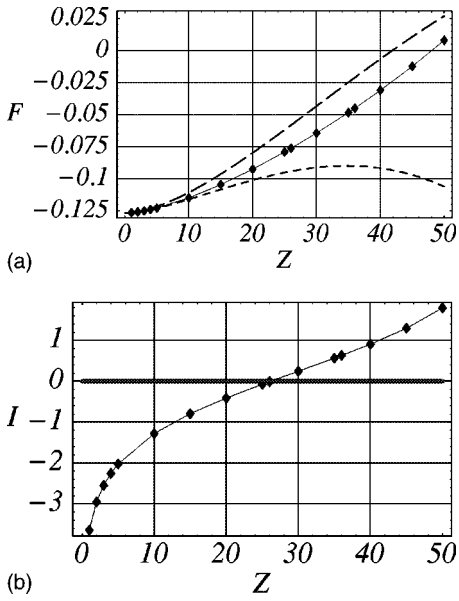

FIG. 7. (a) shows exact and approximate values of the (scaled) self-energy F of a $2P_{1/2}$ electron [see Eq. (1)]. Exact values are given on the solid line. The two-coefficient approximation (41) is represented by long dashes. The three-coefficient approximation (42) uses the value of $A_{60}(2P_{1/2})$, which we provide in Table I, and is indicated by short dashes. (b) displays the improvement provided by the inclusion of A_{60} in the self-energy approximation, as measured by the function I in Eq. (43); negative values of I indicate that including A_{60} improves the approximation.

and the second approximation, $F^{(3)}$, includes in addition the next-order contribution reported in this paper:

$$F^{(3)}(Z\alpha)=A_{40}+(Z\alpha)^2[A_{61}\ln(Z\alpha)^{-2}+A_{60}]. \tag{42}$$

For a given electronic level nl_j, one expects that for low Z, the curve of the higher-order approximation $F^{(3)}(Z\alpha)$ be closer to the curve of $F(Z\alpha)$ than $F^{(2)}(Z\alpha)$. In order to check this, we plotted the quantity

$$I(Z\alpha)=\ln\left|\frac{F(Z\alpha)-F^{(3)}(Z\alpha)}{F(Z\alpha)-F^{(2)}(Z\alpha)}\right|, \tag{43}$$

which should go to $-\infty$ as $Z\to 0$, as can be seen from Eq. (7). In Eq. (43), the purpose of the logarithm is only to obtain more legible graphs; a value of I lower than zero indicates that including A_{60} in the approximation of F improves the lower-order approximation. For the states of Tables I–IV, graphs of Eq. (43) are compatible with their expected behavior [$I(Z\alpha)$ is negative for Z sufficiently close to zero, and is consistent with a $-\infty$ limit]. Figures 7 and 8 show this behavior for two electronic states.

Moreover, the improvement provided by the inclusion of A_{60} in the approximation for F becomes greater as the total angular momentum j increases: for given n and Z, the improvement function (43) decreases as j increases; this behavior can observed by comparing Figs. 7 and 8. Similarily, the range of Z for which approximation $F^{(3)}$ is better than $F^{(2)}$ increases with increasing j. In the worst of the cases consid-

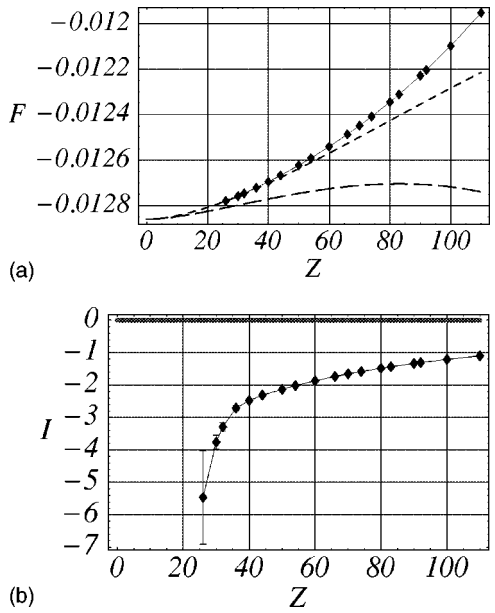

FIG. 8. These two figures represent, respectively, the same quantities as those found in Fig. 7, but for the $5G_{7/2}$ level instead of the $2P_{1/2}$ level. The fact that the curve in (b) contains negative values of I [see Eq. (43)] indicates that the three-order approximation (42) to the self-energy (7) is better than the two-order approximation (41), at least over the range of nuclear charge numbers $Z=25-110$. The three-order approximation (42) uses the value of $A_{60}(5G_{7/2})$ reported in Table IV.

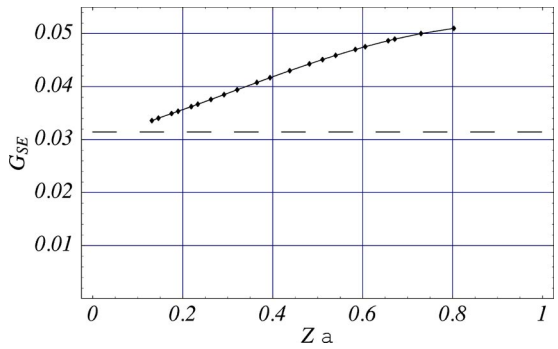

FIG. 9. Plot (solid line) of numerical values of the remainder $G_{\mathrm{SE}}(4D_{5/2},Z\alpha)$ of the self-energy (5); the dashed line indicates the value of $A_{60}(4D_{5/2})\simeq 0.0314$ reported in this paper (see Table II). By definition, the coefficient A_{60} can be obtained as the limit (6) of G_{SE} as $Z\alpha\to 0$. This plot shows that the value of A_{60} extracted from numerical self-energies is consistent with the value obtained by the calculations presented in this paper. We made identical observations for all the states of Tables I–IV.

ered here ($j=1/2$), approximation $F^{(3)}$ is better than $F^{(2)}$ up to $Z\simeq 25$. As shown in Fig. 8, for a high-j level such as $5G_{7/2}$, the higher-order approximation $F^{(3)}$ is better than $F^{(2)}$ even up to $Z=110$.

The second check consisted of estimating A_{60} from the numerical values of the self-energy (1). For all the electronic levels nl_j studied here (except for $8\mathrm{D}_{5/2}$), we have plotted the function $G_{\mathrm{SE}}(nl_j,Z\alpha)$ of Eq. (5); this is made possible by the fact that all the coefficients of Eq. (5) are (analytically) known for any state [3,29], except for the Bethe logarithm which has been numerically evaluated for many states, including the ones we consider here [5,6,41,42]. As indicated in Eq. (6), the limit of the remainder $G_{\mathrm{SE}}(nl_j,Z\alpha)$ as $Z\alpha\to 0$ is by definition $A_{60}(nl_j)$. We have estimated this limit both visually and by fitting $G_{\mathrm{SE}}(nl_j,Z\alpha)$ with various choices of nonzero higher-order terms. A typical curve for $G_{\mathrm{SE}}(Z\alpha)$ is shown in Fig. 9. The estimates of A_{60} obtained by these procedures *confirm* the independent analytic results of Tables I–IV to a typical accuracy of 10–20%, with a few exceptions. Thus, for $2P$ levels, plotting G_{SE} as in Fig. 9 allowed us to confirm the values of $A_{60}(2P_j)$ in Table I to a precision of about 1%. This higher precision is obtained by using the self-energies of $2P$ states obtained in Ref. [15] for values of $Z\alpha$ close to zero ($Z=1,\ldots,5$): such low-Z self-energies are well suited to an evaluation of A_{60} by the limit (6). Plotting G_{SE} for $D_{3/2}$ states lead to $A_{60}(nD_{3/2})=0.005(10)$ for $n=3,\ldots,8$, in agreement with Table II. Finally, since no non-perturbative self-energy (1) is available for $8D_{5/2}$ states, we were not able to independently obtain $A_{60}(8D_{5/2})$ by using such values.

As a by-product of our work with graphs of $G_{\mathrm{SE}}(nl_j,Z\alpha)$, we estimate the self-energy remainder $G_{\mathrm{SE}}(nl_j,\alpha)$ relevant to hydrogen ($Z=1$) to be 0.030(5) for $3D_{5/2}$ and $4D_{5/2}$ states [see Eq. (5)]; this is larger than the estimate of 0.00(1) given in Ref. [2] (p. 468). These two new values change the previous estimate of the self-energy of $3D_{5/2}$ and $4D_{5/2}$ states through Eq. (7) by a relatively large amount, compared to the current best experimental uncertainty in transition frequencies (about 1 Hz [1]). Thus, a variation of 0.03 in $G_{\mathrm{SE}}(3D_{5/2},\alpha)$ in Eq. (5) corresponds to a variation of about 50 Hz in the self-energy correction (1) of the $3D_{5/2}$ level in hydrogen. The same variation in $G_{\mathrm{SE}}(4D_{5/2},\alpha)$ induces a variation of about 20 Hz in the self-energy of the $4D_{5/2}$ level in hydrogen; on the other hand, this change is small compared to the uncertainty of the relevant measurements considered in Ref. [2].

As a third and last check, we used the numerical, exact values of F in order to study the following difference between remainders G_{SE} [see Eqs. (5) and (7)]:

$$\Delta_{\mathrm{fs}}G_{\mathrm{SE}}(nl,Z\alpha)=G_{\mathrm{SE}}(nl_{l+1/2},Z\alpha)-G_{\mathrm{SE}}(nl_{l-1/2},Z\alpha), \tag{44}$$

where, by definition of A_{60} (6),

$$\lim_{Z\alpha\to 0}\Delta_{\mathrm{fs}}G_{\mathrm{SE}}(nl,Z\alpha)=A_{60}(nl_{l+1/2})-A_{60}(nl_{l-1/2}) \tag{45}$$

$$=\Delta_{\mathrm{fs}}A_{60}(nl), \tag{46}$$

which denotes a quantity associated to the fine structure. The numerical evaluation of this limit is interesting: for the states of Tables I–IV, the numerical results for F yield values of $\Delta_{\mathrm{fs}}A_{60}(nl)$ which are more accurate than our numerical estimates of the two individual terms $A_{60}(nl_{l+1/2})$ and $A_{60}(nl_{l-1/2})$. Our analytic values for $\Delta_{\mathrm{fs}}A_{60}$ in Eq. (46) were checked by plotting

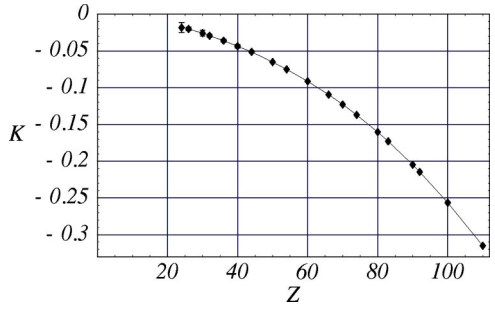

FIG. 10. Plot of the function K in Eq. (47) for the $5F_{7/2}$ and $5F_{5/2}$ states. The limit of this function as $Z\to 0$ must be zero if the coefficients A_{60} of Tables I–IV agree with exact, numerical values of the self-energy. The curve displayed here indicates that the two values of $\Delta_{\rm fs}A_{60}(5F)$ in Eq. (46) obtained independently from Table III and from nonperturbative self-energies (1) [via Eqs. (7), (8), (11c), (44), and (45)] do not differ by more than about 3%.

$$K(Z)=\frac{\Delta_{\rm fs}G_{\rm SE}(nl,Z\alpha)}{\Delta_{\rm fs}A_{60}(nl)}-1, \tag{47}$$

where $\Delta_{\rm fs}G_{\rm SE}(nl,Z\alpha)$ was calculated from the *numerical* values of F [see Eq. (7) and the coefficients reproduced in Sec. II], and where the value of $\Delta_{\rm fs}A_{60}(nl)$ in Eq. (46) was deduced from the *analytic* results of Tables I–IV. If the numerical and analytic estimates of $\Delta_{\rm fs}A_{60}(nl)$ do agree, the function (47) would go to zero as $Z\to 0$. This is indeed consistent with what we observed; Fig. 10 provides an example of this behavior. We *confirm* the values of $\Delta_{\rm fs}A_{60}(nl)$ in Eq. (46) which can be immediately deduced from Tables I–IV. The analytic results for $\Delta_{\rm fs}A_{60}(nl)$ are thus found to be consistent with the numerical data for $\Delta_{\rm fs}G_{\rm SE}$; the level of confirmation is 5–10% [relative to $\Delta_{\rm fs}A_{60}(nl)$] for P and D states (1% for the $2P$ states, and $8D$ states not included, for the reason mentioned above), 3% for F states, and 1% for G states.

This represents an *improvement* over the accuracy of $A_{60}(nl_j)$ obtained by the previous check. This improvement comes evidently from the fact that the relative deviation of $\Delta_{\rm fs}G_{\rm SE}$ in Eq. (44) from $\Delta_{\rm fs}A_{60}$ in Eq. (46) is small over the whole range $0<Z\leqslant 110$, compared to the relative deviation

$$\frac{G_{\rm SE}(nl_j,Z\alpha)}{A_{60}(nl_j)}-1 \tag{48}$$

of $G_{\rm SE}$ [see Eq. (5)] from $A_{60}(nl_j)$ in Eq. (6), with $j=l+1/2$ or $j=l-1/2$. As a consequence, the uncertainty in the numerical evaluation of the limit of Eq. (47) as $Z\to 0$ is relatively small. Figure 10 shows an example of the smallness of the contributions to $\Delta_{\rm fs}G_{\rm SE}$ which go beyond $\Delta_{\rm fs}A_{60}$. Moreover, we have observed that the higher the angular momentum l, the smaller the values of the deviation (47), hence the stronger confirmation of our values of $\Delta_{\rm fs}A_{60}(nl)$ for high orbital angular momenta.

VIII. SUMMARY OF RESULTS

This paper contains results that are relevant to the self-energy of a non-S electron bound to a point nucleus of charge number Z. We provided estimates and values (see also Ref. [9]) for the first two nonanalytically known contributions to the self-energy expansion (5), namely the Bethe logarithm $\ln k_0(nl)$ and the so-called $A_{60}(nl_j)$ coefficient, which can be viewed as a *relativistic* Bethe logarithm. The main numerical results are contained in Tables I–IV, in Eq. (35), and Table VIII, in Eq. (36), and in Eq. (37). We have also conjectured, in Sec. VI, that the order of magnitude of the relativistic Bethe logarithm $A_{60}(nl_j)$ does not depend on the principal quantum number n. In addition to this, we note that the orders of magnitude of $A_{60}(n\,l_{l-1/2})$ and $A_{60}(n\,(l+1)_{l+3/2})$ are the same (for a given set of quantum numbers n and $l>1$) in Tables I–IV. These results, taken together, yield in particular the best available approximations of the self-energy in hydrogen and light hydrogenlike ions, except for $n=1$ and $n=2$ levels [12,15] (see also Sec. VII); such an approximation can be obtained through Eqs. (1) and (7).

Calculating A_{60} has been a challenge since the seminal work of Bethe [4] on the dominant self-energy coefficients of S states [see Eqs. (7) and (1)]. Details of the method we used were described in Secs. III and IV. As discussed in Sec. VII, including the coefficients A_{60} reported in Tables I–IV in a (truncated) expansion of the self-energy improves its accuracy over a large range of nuclear charge numbers Z.

We checked our calculations of A_{60} by both analytic and numerical means. The so-called ϵ method, which we have employed (see Sec. III), makes divergences appear in the low- and high-energy contributions to A_{60}, as the scale-separating parameter ϵ between these two contributions goes to zero. We have observed that, as required, these divergences cancel when the two parts are added. Moreover, our calculations correctly reproduced the known lower-order coefficients A_{40} and A_{61}. We have also checked our results for A_{60} against numerical values of the self-energy, and were able to confirm them by this independent method to the level of about 15% (except for $D_{3/2}$ states, as explained in Sec. VII).

Obtaining results for A_{60} required extending (analytically) the angular algebra developed for $2P$ states [13] to higher angular momenta. Techniques of numerical convergence acceleration of series [7,26,28] were instrumental in evaluating the parts of A_{60} which could not be analytically calculated. The recent analytic calculations of Ref. [27] enabled us to obtain with a high precision the self-energy (1) of electrons with high ($j>3/2$) angular momentum, for various values of the nuclear charge number Z; the new calculations that we have performed required the use of massive parallel computers and thousands of hours of computing time. (These numerical data, which have been used for the plots in Figs. 8–10, will be presented in detail elsewhere [59].) In order to perform numerical checks of A_{60} we have also used the most recent available values of the self-energy. This provided us with independent values of the A_{60} coefficients, extracted from the numerical self-energies, thus allowing us to check the analytic results presented in Tables I–IV (see Sec. VII).

Some cancellations occur between different contributions to A_{60} (in addition to the cancellation of the ϵ-parameter divergences): for some of the atomic states investigated, the absolute magnitude of the A_{60} coefficient is as small as 10^{-3},

whereas the largest individual contribution to A_{60}, when following the classification of the corrections according to Refs. [13,14], is of the order of 10^{-2} or larger for all atomic states discussed here (see also Tables VI and VII).

Future calculations of the Bethe logarithm $\ln k_0(nl)$ and of the relativistic Bethe logarithm $A_{60}(nl_j)$ could also fruitfully be compared to the estimates given by Eqs. (35), (36), and (37), and Table VIII. The results presented in this paper also allow one to perform checks of future exact self-energies obtained by numerical methods, by comparing their values to the three-term self-energy approximation (42) provided here for P and higher-l states. The values of A_{60} in Tables I–IV can be of interest for analyzing the Lamb shift of highly excited (high-n and high-l) electronic states in recent [8,16–18] and future high-precision spectroscopy experiments. The results of Sec. IV–VI also provide the best available self-energy approximation for many states nl_j and nuclear charge numbers Z (see Sec. VII); these approximations can, for instance, be useful in evaluating the contribution of QED effects in atoms [60–63] or molecules [64].

ACKNOWLEDGMENTS

The authors would like to acknowledge helpful discussions with K. Pachucki and J. Sims. We also thank the CINES (Montpellier, France) and the IDRIS (Orsay, France) for grants of time on parallel computers (IBM SP2 and SP3 [50]). E.O.L. acknowledges financial support from the French Ministry of Foreign Affairs, and support by NIST. U.D.J. acknowledges support from the Deutscher Akademischer Austauschdienst (DAAD). G.S. acknowledges support from BMBF, DFG, and from GSI. The Kastler Brossel Laboratory is Unité Mixte de Recherche 8552 of the CNRS.

APPENDIX: LOCAL FITS

This appendix describes a fitting procedure which is designed to extract "*local*" numerical quantities from a set of data points, and to allow one to assess the numerical uncertainty associated to these quantities. A partial sketch of this procedure was first introduced in Ref. [65]. Here, "local" refers, for instance, to the evaluation of a perturbation expansion about one abscissa; the purpose of the method presented here is to perform fits that are local to an abscissa of interest, as opposed to finding the best global fit of some data points. We thus used it in order to obtain asymptotic coefficients for $A_{60}(nl_j)$ for P and D states in Sec. V (see Table VIII), as well as the asymptotic expansion of the Bethe logarithm $\ln k_0(nl)$ in Eq. (37)—in these applications, the quantities evaluated are local to either $n=\infty$ or $l=\infty$. This method can, in principle, be applied to many other problems that require local fits.

In order to describe the local-fit procedure, we take the evaluation of the limit

$$\lim_{l\to\infty} l^3 \ln k_0(\overline{nl}) \tag{A1}$$

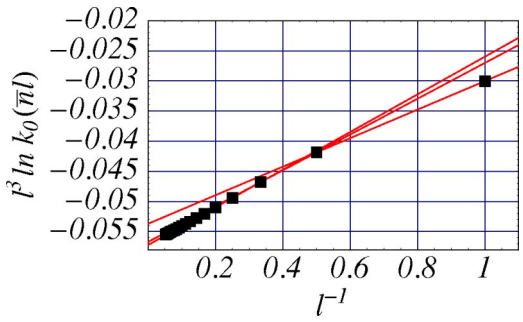

FIG. 11. This figure shows the lines going through a few pairs of successive data points given by (A2)—see also Fig. 2. Each of these lines is a local approximation to the curve underlying the data points. Each line yields an estimate of limit (A1) of the data points as $l^{-1}\to 0$ (this estimate is at the intersection of the line with the $l^{-1}=0$ axis). Figure 12 graphically displays these estimates.

as an example—here we have $\overline{n}=l+1$ and $\ln k_0(nl)$ is the Bethe logarithm (9). This limit was evaluated as $-0.056\,853(2)$ [see Fig. 2 and Eq. (37)].

Figures 2 and 11 contain data points which are relevant to Eq. (A1): we have plotted

$$l^3 \ln k_0(\overline{nl}) \tag{A2}$$

as a function of l^{-1} (with values of the Bethe logarithm found in Ref. [6]). The limit (A1) can visually be estimated from the data points in Fig. 2 to be $-0.057(1)$.

In order to improve over the estimate $-0.057(1)$ for Eq. (A1), we fit (exactly) each pair of two consecutive points (A2) in Fig. 2 with a line, as depicted in Fig. 11. Each of the fitting lines in Fig. 11 gives an estimate of limit (A1) by extrapolation to $l^{-1}=0$ (intersection of the line with the $l^{-1}=0$ axis). Figure 12 contains each of these estimates, as a function of the average abscissa of the two points that were

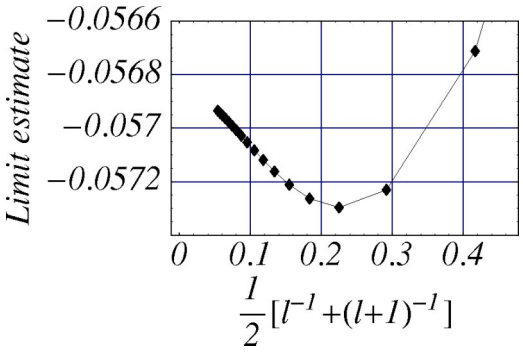

FIG. 12. This figure shows the estimates of limit (A1) obtained through the two-point fits of Fig. 11. From this graph, we estimate limit (A1) to be $-0.0568(1)$, which is more precise than, and consistent with the value $-0.057(1)$ obtained from the original data in Figs. 2 and 11. The limit estimates are plotted along the vertical direction, while the abscissa associated to an estimate is the average abscissa of the two data points of Fig. 11 which were used in producing it.

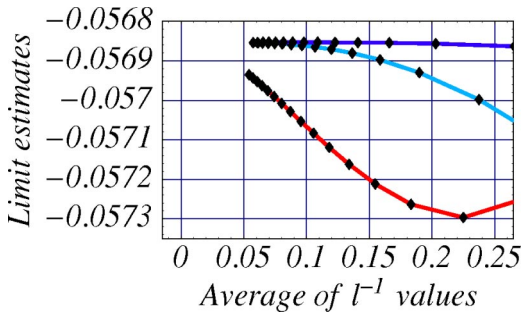

FIG. 13. From the lower to the higher curve: estimates of limit (A1) obtained through fits of the data points given by (A2) with polynomials of degree 1 (see also Fig. 12), 3, and 5 (see also Fig. 14). Fitting the data in Fig. 11 with 1–6 points yielded mutually coherent estimates of limit (A1) with an exponentially decreasing error.

used in obtaining it. Because the curve in Fig. 12 is relatively flatter than the curve in Fig. 11, we can estimate limit (A1) with an improved uncertainty; thus, we deduce from Fig. 12 the value $-0.0568(1)$ for limit (A1) that we are studying, which is consistent with the previous estimate $-0.057(1)$.

This better estimate $-0.0568(1)$ of limit (A1) can be further improved by continuing to increase the number p of data points (A2) included in local fits of the data. Thus, for an increasing number p of data points, we fitted (exactly) each set of p successive points (A2) in Fig. 11 with a polynomial of degree $p-1$ (linear combination of the functions 1, $l^{-1}, \ldots, l^{-(p-1)}$) and represented the value of the polynomial extrapolated to $l^{-1}=0$ as a function of the average abscissa of the p points. Figure 13 depicts this process. The plotted values are estimates of limit (A1) obtained with higher and higher-order (local) fits of the data points given by (A2). In Fig. 13, the abscissa of each estimate is the average of the abscissas l^{-1} of the fitted data points given by (A2). We observed that the curves so obtained become *exponentially flat*, in the sense that their relative amplitudes become exponentially smaller and smaller—until the uncertainties of individual estimates become important, as described below. This fact, which is illustrated in Fig. 13, allowed us to obtain more and more accurate estimates of limit (A1).

The most accurate value that we obtained for limit (A1) through the local-fit procedure described here is $-0.056\,853(2)$ [see Eq. (37)], as is illustrated in Fig. 14. This limit was obtained by fitting each sequence of $p=6$ data points with a fifth-degree polynomial. Fits of the data points (A2) with larger numbers of data points display more irregular estimate curves; this can, for instance, be seen by comparing Fig. 14 with Fig. 15.

As we have seen above, the uncertainty in the fitted value can be evaluated by visually extrapolating the fitting curves (i.e., curves such as those of Figs. 12–15). Another uncertainty must in general be taken into account in order to obtain a reliable estimate for the fitted quantity: the uncertainty in the data points. All the curves presented in this appendix do contain error bars that reflect the uncertainties in the estimates of Eq. (A1), which come from the uncertainties in the data points given by (A2). We evaluated the uncertainty

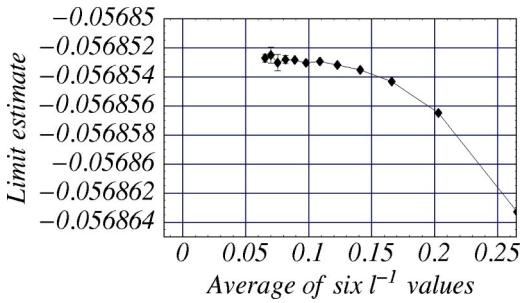

FIG. 14. This figure shows estimates of limit (A1) obtained by fitting the data in Fig. 11 with fifth-degree polynomials (in l^{-1}). The high relative stability of the estimates as $l^{-1}\to 0$ allowed us to give the precise value $-0.056\,853(2)$ in Eq. (37) for limit (A1).

associated to each fit of p data points given by (A2) by calculating three fits: a fit with the middle values of the ordinates, a fit with the higher values, and a fit with the lower values; the three estimates of the fitted quantity (A1) obtained through this procedure define an estimate with an error bar (see, e.g., Fig. 15). Other ways of estimating the uncertainty in the fit result can be used; a good choice of uncertainty evaluation yields successive estimates of the fitted quantity which are compatible with a smooth curve of estimates (see, e.g., Fig. 15).

One of the advantages of the local-fit method presented in this appendix is that data points that are located far from the abscissa of interest ($l^{-1}=0$, here) can fruitfully be used in evaluating the fitted quantity [limit (A1), in our example]. Thus, as Fig. 15 illustrates, data points given by (A2) with ''large'' abscissas can yield more precise estimates of limit (A1) than data points with small abscissas. This behavior is particularly useful when data points in the region of interest have relatively large uncertainties.

The procedure detailed in this appendix also allows one to study the quality of lists of numerical results that should lie on a smooth curve, but whose consistency is not obvious through a simple inspection or plot of the values. In fact,

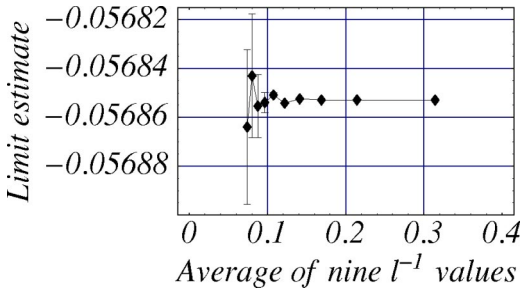

FIG. 15. This figure displays estimates of limit (A1) obtained by fitting the data in Fig. 11 with a eigth-degree polynomials (in l^{-1}). It should be compared to Fig. 14, which gives a more accurate estimate of limit (A1) by fitting sequences of only six data points. The accuracy of the local fits performed here first increases with the order of the local approximations to the data points given by (A2) (see Fig. 13) and then eventually decreases (compare this plot to Fig. 14).

curves such as those found in Figs. 12–15 can be very sensitive to small errors in a list of numerical values. We have not noticed such errors in the A_{60} values of Tables I and II while evaluating the asymptotic coefficients reported in Table VIII; this provided an additional check of the values reported in these tables (see also Sec. VII).

The local-fit method described here is not restricted to the asymptotic study of the Bethe logarithm that we have used as an example. In general, it can yield precise estimates of quantities that are local to a set of data point [such as limit (A1)], including, for instance, perturbation coefficients of nonanalytic expansions [e.g., Eq. (5)].

[1] F. Biraben *et al.*, in *The Hydrogen Atom: Precision Physics of Simple Atomic Systems*, edited by S.G. Karshenboim, F.S. Pavone, F. Bassani, M. Inguscio, and T.W. Hänsch, Lecture Notes in Physics Vol. 270 (Springer, New York, 2001), p. 17.

[2] P.J. Mohr and B.N. Taylor, Rev. Mod. Phys. **72**, 351 (2000).

[3] G.W. Erickson and D.R. Yennie, Ann. Phys. (N.Y.) **35**, 271 (1965).

[4] H.A. Bethe, Phys. Rev. **72**, 339 (1947).

[5] S.P. Goldman and G.W.F. Drake, Phys. Rev. A **61**, 052513 (2000).

[6] G.W.F. Drake and R.A. Swainson, Phys. Rev. A **41**, 1243 (1990); the quantity denoted by $\ln[k_0(nl)/R_\infty]$ in this reference is written $\ln[k_0(nl)]$ in the present paper.

[7] S.V. Aksenov, M.A. Savageau, U.D. Jentschura, J. Becher, G. Soff, and P.J. Mohr, Comput. Phys. Commun. **150**, 1 (2003).

[8] J.C. DeVries, Ph.D. thesis, MIT, 2002 (unpublished).

[9] U.D. Jentschura, E.-O. Le Bigot, P.J. Mohr, P. Indelicato, and G. Soff, Phys. Rev. Lett. **90**, 163001 (2003).

[10] K. Pachucki, Phys. Rev. A **46**, 648 (1992).

[11] K. Pachucki, Ann. Phys. (N.Y.) **226**, 1 (1993).

[12] U.D. Jentschura, P.J. Mohr, and G. Soff, Phys. Rev. Lett. **82**, 53 (1999).

[13] U. Jentschura and K. Pachucki, Phys. Rev. A **54**, 1853 (1996).

[14] U.D. Jentschura, G. Soff, and P.J. Mohr, Phys. Rev. A **56**, 1739 (1997).

[15] U.D. Jentschura, P.J. Mohr, and G. Soff, Phys. Rev. A **63**, 042512 (2001).

[16] B. de Beauvoir, F. Nez, L. Julien, B. Cagnac, F. Biraben, D. Touahri, L. Hilico, O. Acef, A. Clairon, and J.J. Zondy, Phys. Rev. Lett. **78**, 440 (1997).

[17] C. Schwob, L. Jozefowski, B. de Beauvoir, L. Hilico, F. Nez, L. Julien, F. Biraben, O. Acef, and A. Clairon, Phys. Rev. Lett. **82**, 4960 (1999).

[18] C. Schwob, L. Jozefowski, B. de Beauvoir, L. Hilico, F. Nez, L. Julien, F. Biraben, O. Acef, J.-J. Zondy, and A. Clairon, Phys. Rev. Lett. **86**, 4193 (2001).

[19] J. Reichert, M. Niering, R. Holzwarth, M. Weitz, T. Udem, and T.W. Hänsch, Phys. Rev. Lett. **84**, 3232 (2000).

[20] M. Niering *et al.*, Phys. Rev. Lett. **84**, 5496 (2000).

[21] B. de Beauvoir, C. Schwob, O. Acef, L. Jozefowski, L. Hilico, F. Nez, L. Julien, A. Clairon, and F. Biraben, Eur. Phys. J. D **12**, 61 (2000).

[22] P.J. Mohr, G. Plunien, and G. Soff, Phys. Rep. **293**, 227 (1998).

[23] P. Indelicato and P.J. Mohr, Phys. Rev. A **58**, 165 (1998).

[24] P.J. Mohr, Ann. Phys. (N.Y.) **88**, 26 (1974).

[25] P.J. Mohr, Ann. Phys. (N.Y.) **88**, 52 (1974).

[26] U. D. Jentschura, *Quantum Electrodynamic Radiative Corrections in Bound Systems*, Dresdner Forschungen: Theoretische Physik, Band 2 (w.e.b. Thelem, Universitätsverlag, Dresden, 1999).

[27] E.-O. Le Bigot, P. Indelicato, and P.J. Mohr, Phys. Rev. A **64**, 052508 (2001).

[28] U.D. Jentschura, P.J. Mohr, G. Soff, and E.J. Weniger, Comput. Phys. Commun. **116**, 28 (1999).

[29] G.W. Erickson and D.R. Yennie, Ann. Phys. (N.Y.) **35**, 447 (1965).

[30] G.W. Erickson, Phys. Rev. Lett. **27**, 780 (1971).

[31] J. Sapirstein, Phys. Rev. Lett. **47**, 1723 (1981).

[32] S.G. Karshenboim, Z. Phys. D: At., Mol. Clusters **39**, 109 (1997).

[33] J. Sapirstein and D. R. Yennie, *Quantum Electrodynamics* (World Scientific, Singapore, 1990), pp. 560–672.

[34] H.A. Bethe and E.E. Salpeter, *Quantum Mechanics of One-and Two-electron Atoms* (Spring-Verlag, Berlin, 1957); the quantity denoted by $\ln\{K_0(nl)/[Z^2\mathrm{Ry}]\}$ in this reference is written $\ln[k_0(nl)]$ in the present paper.

[35] S. Klarsfeld and A. Maquet, Phys. Lett. **43B**, 201 (1973).

[36] H.A. Bethe, L.M. Brown, and J.R. Stehn, Phys. Rev. **77**, 370 (1950).

[37] J.M. Harriman, Phys. Rev. **101**, 594 (1956).

[38] C. Schwartz and J.J. Tieman, Ann. Phys. (N.Y.) **6**, 178 (1959).

[39] M. Lieber, Phys. Rev. **174**, 2037 (1968).

[40] R.W. Huff, Phys. Rev. **186**, 1367 (1969).

[41] R.C. Forrey and R.N. Hill, Ann. Phys. (N.Y.) **226**, 88 (1993).

[42] S.E. Haywood and J.D. Morgan III, Phys. Rev. A **32**, 3179 (1985).

[43] *Handbook of Mathematical Functions*, edited by M. Abramovitz and I. A. Stegun, 9th ed. (Dover, New York, 1972).

[44] K. Pachucki, Phys. Rev. A **48**, 2609 (1993).

[45] U.D. Jentschura and K. Pachucki, J. Phys. A **35**, 1927 (2002).

[46] E.H. Wichmann and C.H. Woo, J. Math. Phys. **2**, 178 (1961).

[47] L. Hostler, J. Math. Phys. **11**, 2966 (1970).

[48] A.R. Edmonds, *Angular Momentum in Quantum Mechanics* (Princeton University Press, Princeton, NJ, 1957).

[49] S. Wolfram, *Mathematica—A System for Doing Mathematics by Computer* (Addison-Wesley, Reading, MA, 1988).

[50] Certain commercial equipment, instruments, or materials are identified in this paper to foster understanding. Such identification does not imply recommendation or endorsement by the National Institute of Standards and Technology, nor does it imply that the materials or equipment identified are necessarily the best available for the purpose.

[51] F.W.J. Olver, *Asymptotics and Special Functions* (Academic Press, New York, 1974).

[52] H. Bateman, *Higher Transcendental Functions* (McGraw-Hill, New York, NY, 1953), Vol. 1.

[53] E.J. Weniger, Comput. Phys. Rep. **10**, 189 (1989).

[54] G.W. Erickson, J. Phys. Chem. Ref. Data **6**, 831 (1977).
[55] S. Kotochigova, P.J. Mohr, and B.N. Taylor, Can. J. Phys. **80**, 1373 (2002).
[56] P.J. Mohr and Y.-K. Kim, Phys. Rev. A **45**, 2727 (1992).
[57] P.J. Mohr, Phys. Rev. A **46**, 4421 (1992).
[58] P. Indelicato and P.J. Mohr, Hyperfine Interact. **114**, 147 (1998).
[59] É.-O. Le Bigot, U.D. Jentschura, P.J. Mohr, and P. Indelicato (unpublished).
[60] U. Feldman, J. Sugar, and P. Indelicato, J. Opt. Soc. Am. B **8**, 3 (1990).
[61] F. Parente, J.P. Marques, and P. Indelicato, Europhys. Lett. **26**, 437 (1994).
[62] D.R. Beck, Phys. Rev. A **56**, 2428 (1992).
[63] J. Sugar, V. Kaufman, P. Indelicato, and W.L. Rowan, J. Opt. Soc. Am. B **6**, 1437 (1989).
[64] P. Pyykkö, K.G. Dyall, A.G. Császár, G. Tarczay, O.L. Polyansky, and J. Tennyson, Phys. Rev. A **63**, 024502 (2001).
[65] P.J. Mohr, Phys. Rev. Lett. **34**, 1050 (1975).